Chemical Physics 485–486 (2017) 98–107

Contents lists available at ScienceDirect

Chemical Physics

journal homepage: www.elsevier.com/locate/chemphys

Piezoelectric, elastic, Infrared and Raman behavior of ZnO wurtzite under pressure from periodic DFT calculations

Naiara Letícia Marana [a], Silvia Maria Casassa [b], Julio Ricardo Sambrano [a,*]

[a] Modeling and Molecular Simulations Group, São Paulo State University, UNESP, 17033-360 Bauru, SP, Brazil
[b] Theoretical Group of Chemistry, Chemistry Department, Torino University, Torino, Italy

ARTICLE INFO

Article history:
Received 11 November 2016
In final form 1 February 2017
Available online 3 February 2017

ABSTRACT

The influence of pressure on elastic, piezoelectric (total and clamped-ion contribution), dielectric constants, Infrared and Raman spectra, and topological properties of ZnO wurtzite structure was carried out via periodic DFT/B3LYP methodology. The computational simulation indicated that, as the pressure increases, the structure becomes more rigid and an enhancement of the direct piezoelectric response along the *z*-direction was observed. Bader topological analysis and Hirshfeld-I charges showed a slight increase in the ionic character of Zn–O bond. Besides that, changes in the piezoelectric response are mainly due to the approach between Zn and O than to charge transfer phenomena among the two atoms. Pressure induces a sensitive displacement in the Infrared and Raman frequencies and a decrease of the E_2 mode. Nevertheless, the increase of pressure does not lead to a change in the semiconductor character, which proves that the ZnO support high pressures and can be applied in different devices.

1. Introduction

Zinc Oxide (ZnO) is a typical II-VI type semiconductor mainly found in the hexagonal wurtzite (W) structure. This phase has a direct band gap (~3.37 eV) [1] and the highest piezoelectric tensor among the tetrahedral bonded semiconductors [2]. Its properties are extremely important in energy harvesting, particularly in photovoltaics [3–7], piezoelectric nanogenerators [8–11], hydrogen fuel generation [12], thin film piezoelectric devices [13], such as bulk acoustic wave and surface acoustic wave resonators, filters, sensors, and microelectromechanical systems. This material has received great attention from both the theoretical [14–17] and experimental [13–18] point of view due to its immense variety of applications which mostly exploit its piezoelectric properties.

Kumar and Kim [19] report on several applications and researches on nanostructures based on ZnO due to its high piezoelectric character, such as solar energy harvesting, dye-sensitized solar cells, bulk hetero-junction organic solar cells, and others.

Catti et al. [14] analyzed the elastic and piezoelectric constants of W-ZnO and W-ZnS and showed that the piezoelectric constants of ZnO are always much higher than those of ZnS as a result of two properties (i) the relaxation coefficient which is smaller in ZnO and (ii) the unit-cell edge is larger for ZnS.

Parallel to the piezoelectric constants, the study of elastic properties as stiffness, Young's and bulk modulus and yield strength has drawn the attention of the scientific community motivated by their direct relationship with piezoelectricity and possible applications resulting from the understanding of chemical bonds and cohesion within a material.

ZnO elastic and piezoelectric constants have been studied relating to temperature [20], with different theoretical methods [16,21,22] and results have been compared with that obtained from other piezoelectric materials [23]. Moreover, there are many works about ZnO structural, electrical and vibrational properties and performances as a function of pressure [24–26]. However, as far as we know, there are no studies about the influence of pressure on elastic, piezoelectric and dielectric constants.

Accordingly to that, a computational study is carried out based on density functional theory (DFT) applied to a periodic model of the W-ZnO crystal in order to investigate the influence of pressure on total and clamped-ion contributions to the, elastic and piezoelectric constants, dielectric constants, electronic structure and on the Infrared (IR) and Raman spectra. In particular, changes in the electron density, $\rho(\mathbf{r})$, were monitored through the analysis of topological properties according to QTAIMAC [27,28] and Hirshfeld-I [29] charges were also calculated for the first time using the CRYSTAL program.

* Corresponding author.
E-mail address: sambrano@fc.unesp.br (J.R. Sambrano).

http://dx.doi.org/10.1016/j.chemphys.2017.02.001
0301-0104/

2. Models and computational methods

2.1. Computational method

The calculations were performed at the periodic DFT level, adopting the B3LYP [30,31] hybrid functional as implemented in the CRYSTAL14 software [32]. CRYSTAL uses a Gaussian-type basis set to represent crystalline orbitals as a linear combination of Bloch functions defined in terms of local functions (atomic orbitals). The zinc and oxygen atoms were described by all-electrons 86-411d31G [33] and 8-411d1G [34] basis sets respectively, which have been used in previous investigations [35–37] and have provided the best approximation to the experimental band gap energy, lattice and internal parameters.

DFT integration was performed on an *extra-extra-large* grid [38] containing 99 radial points and 1454 angular points, respectively. The accuracy of the truncation criteria for bi-electronic integrals is controlled by a set of five thresholds whose values were set to: 10^{-8}, 10^{-8}, 10^{-8}, 10^{-8} and 10^{-16}. The shrinking factor for both the Pack-Monkhorst and Gilat net was set to 4, corresponding to 12 independent k points in the irreducible part of the Brillouin zone.

All structures were optimized by the use of analytical energy gradients with respect to atomic coordinates and unit cell parameters. Convergence was checked on gradient components and nuclear displacements with tolerances on their root mean square set to 0.0003 and 0.0012 a.u., respectively.

The electronic properties were analyzed by computing the total (DOS), projected density of states (PDOS) and the band structure diagrams. The shift of the IR and Raman frequencies under pressure were also studied. The vibrational frequencies at the Γ point were computed within the harmonic approximation by diagonalizing the mass-weighted Hessian matrix of the second derivatives of the total energy per cell with respect to pair of atomic displacements in the reference cell. More details on the computational vibrational frequencies scheme can be found in [39].

The topological analysis of $\rho(\mathbf{r})$ was done with the TOPOND code [40] especially suited for crystalline systems [28] and recently incorporated in the CRYSTAL14 package. The theoretical details can be found in articles expressly devoted to the topological analysis [41,42]. This work focused on the determination and characterization of the bond critical points (BCP) corresponding to (3,−1) points in the Bader notation, of the charge density in order to envisage the effect of pressure on the Zn–O interaction.

Bader and Hirshfeld-I [29] methods perform a partition of the physical observable electron density to define atoms in molecules and crystals and consequently determine their charge. Bader's QTAIM defines atomic basins as those surrounded by zero-flux surfaces and $\rho(\mathbf{r})$ is integrated within these regions with an accuracy controlled by few input parameters. The stockholders partition by Hirshfeld dissects the system into well-defined atomic fragment and the integration of $\rho(\mathbf{r})$ is weighted according to a general and natural choice that is to share the charge density at each point among several atoms in proportion to their free-atom densities, at the corresponding distances from the nuclei [38]. The Hirshfeld-I method, which has renewed the interest in the original Hirshfeld scheme [43], eliminates the need of calculating the promolecular density by replacing them with spherical symmetric weight functions, optimized through an iterative procedure. Its extension to periodic systems has been recently implemented [44] in the development version of the CRYSTAL program.

2.2. Elastic and piezoelectric constants

Elastic constants are the second derivatives of the total energy, E, with respect to the strain along two crystallographic directions:

$$\boldsymbol{C_{vu}} = \frac{1}{\boldsymbol{V}} \frac{\partial^2 \boldsymbol{E}}{\partial \boldsymbol{\mu_v} \boldsymbol{\mu_u}} \tag{1}$$

in the formula above, V is the equilibrium unit cell volume, $\boldsymbol{\mu_u}$ and $\boldsymbol{\mu_v}$ are the components of the symmetric second-rank pure strain tensor [45] and Voigt's notation is used according to which u, $v = 1, 2, \ldots, 6$ (1 = xx, 2 = yy, 3 = zz, 4 = yz, 5 = xz, 6 = xy). In the CRYSTAL package, an automated scheme was implemented for the calculation of $\boldsymbol{C}$ and its compliance tensor, $\mathbb{S} = \boldsymbol{C}^{-1}$, that exploits the analytical gradients and computes the second derivatives numerically [22,46].

In the linear regime of the response theory, *direct* ($\boldsymbol{e}$) and *converse* ($\boldsymbol{d}$) piezoelectric tensors describe the polarization ($\boldsymbol{P}$) induced by strain ($\boldsymbol{\mu}$) at constant electric field (ε) and the strain induced by an external electric field at constant stress ($\boldsymbol{\sigma}$), respectively:

$$\boldsymbol{P} = \boldsymbol{e\mu} \tag{2}$$

$$\boldsymbol{\mu} = \boldsymbol{d\varepsilon} \tag{3}$$

The computational approach consists in directly computing the intensity of the polarization induced by the strain, so that each piezoelectric stress coefficients can be written as:

$$\boldsymbol{e}_{iv} = \left(\frac{\partial P_i}{\partial \mu_v}\right)_{\varepsilon} \tag{4}$$

in the above expression $i = x$, y or z and the derivative is calculated at constant electric field. In the present work, the polarization was computed via Berry phase (BP) approach [47] as implemented in CRYSTAL [21] and according to Eq. (4) can be recasted in terms of the BP $\{\varphi_l\}$:

$$\boldsymbol{e_{iv}} = \frac{|e|}{2\pi V} \sum_{li} a_{li} \frac{\partial \varphi_l}{\partial \mu_v} \tag{5}$$

where $\boldsymbol{a_{li}}$ is the $\boldsymbol{i}$th Cartesian component of the $\boldsymbol{l}$th direct lattice basis vector $\boldsymbol{a_l}$ and the derivative is calculated numerically by applying finite strains to the crystal lattice. Finally, a simple connection exists between the *direct* and *converse* piezoelectric tensors:

$$\boldsymbol{d} = \boldsymbol{e}\mathbb{S} \tag{6}$$

that can be exploited to computed $\boldsymbol{d}$.

The macroscopic piezoelectric constants can be separated in two components: electronic "clamped-ion" and nuclear "internal strain" contributions, i.e., $\boldsymbol{e_{iv}} = \boldsymbol{e_{iv}^{clamp}} + \boldsymbol{e_{iv}^{nuclear}}$. The nuclear term measures the piezoelectric effect due to an internal microscopic strain [48]. For details about the numerical accuracy of elastic and piezoelectric calculations with the CRYSTAL program, see references [14,22] and [49].

2.3. ZnO structure

The ZnO structure belongs to the point group $P6_3mc$, with a Bravais lattice (a = 3.250 Å and c = 5.207 Å, u = 0.382) [50]. The unit cell has two units of ZnO, with a $[ZnO_4]$ tetrahedron depicted as alternating planes of tetrahedrally coordinated oxygen and Zn atoms, stacked alternatively along the c-axis (see reference [51]). Its spectrum is characterized by $2E_2 + 2E_1 + 2A + 2B_1$, where the E_1, E_2, and A modes are active in Raman scattering and the E_1 and A_1 modes are active in IR. B_1 are "silent modes" [52].

In this structure, there are five elastic constants, C_{11}, C_{12}, C_{13}, C_{33} and C_{44} (see Ref. [53]) and three independent non-zero piezoelectric stress coefficients, e_{31}, e_{33} and e_{15}. The elastic constants can be further divided into two groups: diagonal terms (directly related to the second derivative of the energy, independent constant) represented by the constants C_{11}, C_{33} and C_{44}, and off-diagonal terms

(the second derivative is obtained by deformation of two terms; dependent constant) represented by C_{12} and C_{13}.

The elastic constants C_{44} affects all unit cell parameters and then can be interpreted as a shear constant corresponding to the transversal mode in direction [0001] and [1000]. C_{13} is the combination of four velocity modes of propagation in [0011].

The CRYSTAL code calculated the bulk modulus through a linear combination of elastic constants, $B = \frac{1}{9}[(C_{11} + C_{22} + C_{33}) + 2(C_{12} + C_{13} + C_{23})]$ [22]. For more details see references [22,53] and [54].

3. Results and discussions

3.1. Structural properties

The cell (a and c) and internal (u) optimized parameters are in good agreement with available experimental data, [50,55] with a deviation of 0.57%, 0.20%, and 0.26%, respectively, see Table 1. It is noteworthy that, at room temperature, the transition phase of wutzite to rocksalt is observed near 9 GPa [25], however, the rocksalt stability phase is up to 56.6 GPa [56]. Therefore, different pressures, ranging from zero to 12.5 GPa (P = 0.0, 2.5, 5.0, 7.5, 10.0, 12.5 GPa) were applied on the optimized zero-pressure structure and for each of them a symmetry constrained geometry relaxation was performed.

Elastic and piezoelectric constants were determined for each equilibrium geometry under pressure. The structural parameters, volume, elastic constants and band gap energy results are summarized in Table 1 and the linear dependency of the various quantities as a function of pressure are presented in Fig. 1. As a general comment, the cell parameter a and c are more sensitive to the deformation than the internal parameter u (Fig. 1a).

The ratio c/a = 1.597 at 0 GPa is the same calculated at 7.5 GPa and 12.5 GPa and it is 0.004 and 0.036 lower than that of the experimental [50] and ideal structure, respectively, and this demonstrates that the symmetry is maintained during the loading process. Both the cell parameters reduce linearly in function of pressure with a decrease of 0.08 Å (−2.44%) and 0.13 Å (−2.48%) respectively in the crystal at 12.5 GPa. As a consequence, the cell volume contracts 4.49% at 7.5 GPa and 6.99% at 12.5 GPa. The internal parameter u shows an opposite trend with an increase of the ∼0.26% at the maximum pressure.

3.2. Elastic constants

At 0 GPa, the calculated elastic constants are in good agreement with experimental and theoretical literature values, as can be seen in Table 1. Differences are in the order of 4.81%, 4.20%, 1.92%, 3.72%, −2.22% and 3.49% for C_{11}, C_{12}, C_{13}, C_{33}, C_{44} and bulk modulus, respectively, from the experimental data [57]. Therefore, this computational setup is able to reproduce, with good precision, the structural parameter and to properly estimate the forces acting on the system.

As regards W-ZnO elastic properties, total and clamped-ion, the high value of $C_{33} \equiv zzzz$ indicates that the structure is more rigid along the z-direction, whereas along the $C_{44} \equiv yzyz$ and $C_{13} \equiv xxzz$ directions the crystal is softer. Furthermore, the zinc along to the z-direction is most symmetry-constrained than the oxygen atoms, while both atoms can be moved easier in the yz and xz planes.

As the pressure is applied, the relaxed elastic constants C_{11}, C_{12}, C_{13} and C_{33} showed a linear increase (Fig. 1b) which leads to a more rigid structure, as confirmed by the increment of the bulk modulus. On the contrary, the elastic constant C_{44} presents an opposite behavior indicating that the structure is the softest and tends to shear in that direction. In the pressure range near the experimental phase transition [56], the variations for C_{11}, C_{12}, C_{13}, C_{33}, and C_{44} are the following: 11.01%, 29.03%, 33.02%, 9.42% and −11.36% at 7.5 GPa and 13.76%, 37.90%, 45.28%, 12.10% and −13.63% at 10.0 GPa. Thus, the maximum change occurs for the C_{13} and C_{12} constants and the minimum for the C_{44} constant.

Under pressure, all clamped-ion elastic constants demonstrated an increase behavior. The C_{11}, C_{33} and C_{44} show an increase in their

Table 1
Cell (a and c, Å) and internal parameter (u), volume (V, Å^3), elastic constants (C_{ij}, GPa), bulk modulus (B, GPa), and band gap energy (E_{gap}, eV) of W-ZnO without and under pressure (P, GPa) to the total and electronic clamped-ion contribution.

P	a	c	u	V	C_{11}	C_{12}	C_{13}	C_{33}	C_{44}	B	E_{gap}
					Total						
0.0	3.28	5.24	0.383	48.73	218	124	106	223	44	148	3.21
2.5	3.26	5.21	0.383	47.93	226	137	117	231	42	159	3.25
5.0	3.24	5.19	0.383	47.21	233	147	130	238	41	169	3.29
7.5	3.23	5.16	0.383	46.54	242	160	141	244	39	179	3.33
10.0	3.21	5.13	0.384	45.91	248	171	154	250	38	189	3.36
12.5	3.20	5.11	0.384	45.32	257	183	164	255	36	199	3.40
					Clamped-ion						
0.0	3.28	5.24	0.383	48.73	284	95	68	302	59	148	3.21
2.5	3.26	5.21	0.383	47.93	303	104	74	323	61	159	3.25
5.0	3.24	5.19	0.383	47.21	320	112	80	345	62	170	3.29
7.5	3.23	5.16	0.383	46.54	337	121	85	361	64	180	3.33
10.0	3.21	5.13	0.384	45.91	354	129	91	380	65	190	3.36
12.5	3.20	5.11	0.384	45.32	373	139	97	400	66	201	3.40
					0.0 GPa						
Exp.	3.26[a]	5.22[a]	0.382[a]	47.98[a]	208[b]	119[b]	104[b]	215[b]	45[b]	183	3.37[c]
Exp.	3.25[d]	5.21[d]	–	47.62[d]	–	–	–	–	–	143[e]	–
The.	3.29[f]	5.24[f]	0.383[f]	–	246[f]	127[f]	105[f]	246[f]	56[f]	160[g]	–
The.	3.29[h]	5.28[h]	0.382[h]	–	217[h]	115[h]	95.2[h]	224[h]	44[h]	–	3.23[h]

[a] [50].
[b] [57].
[c] [58].
[d] [56].
[f] [14].
[g] [59].
[h] [17].

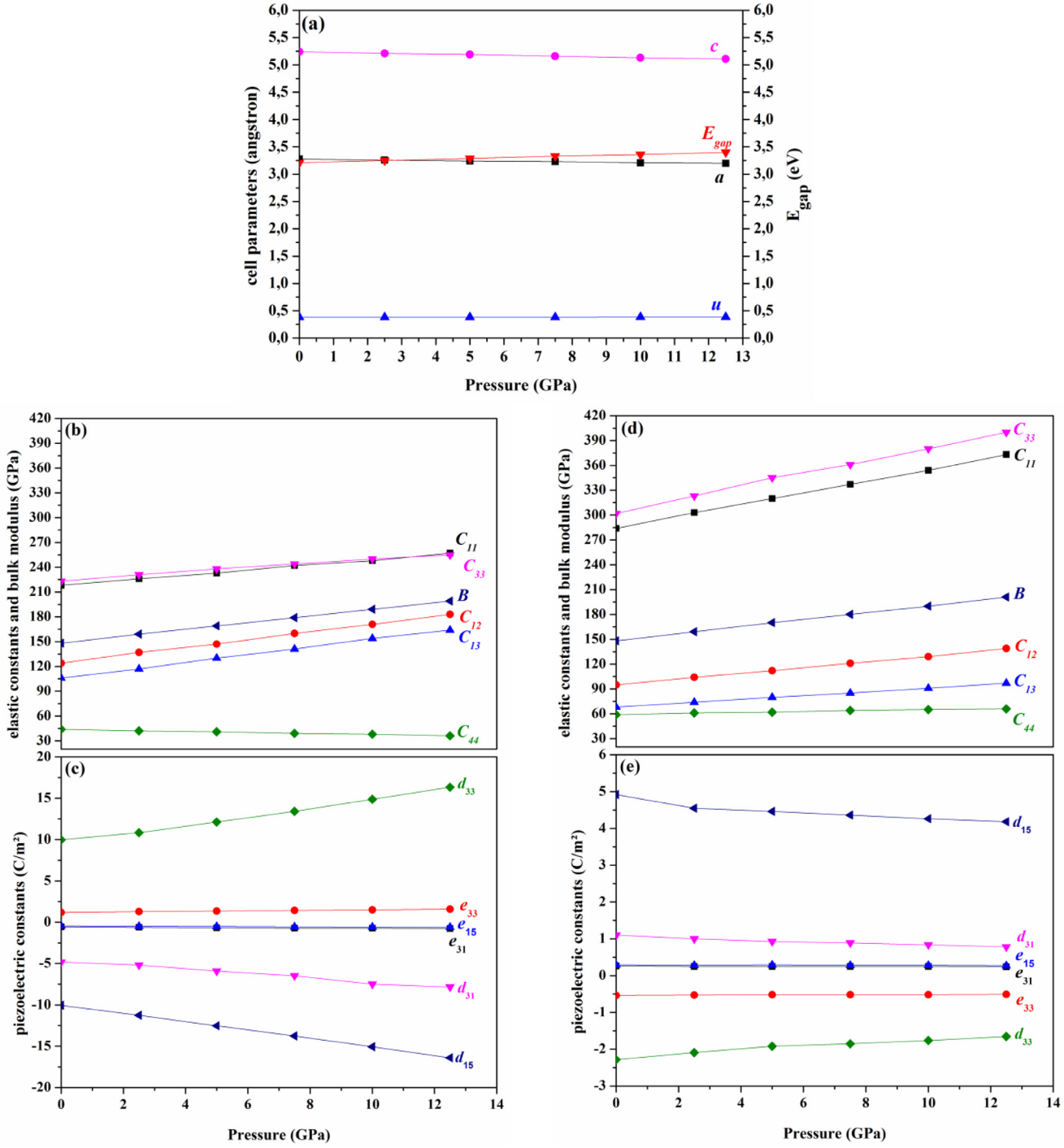

Fig. 1. (a) Cell parameters and E_{gap}, (b) elastic and (c) piezoelectric constants of total contribution, (d) elastic and (e) piezoelectric constants of clamped-ion contribution.

values with respect to the total elastic constants, in average, 37.8%, 46.2% and 58%, respectively; while the C_{12} and C_{13} presented a decrease of 31.8% and 63.5%, respectively. However, besides the differences between the total and clamped-ion, the bulk modulus values kept almost unchanged.

At 12.5 GPa, the elastic constants present a variation of 39, 59, 58, 32, and -8 GPa, for C_{11}, C_{12}, C_{13}, C_{33}, and C_{44}, respectively. This trend shows that the C_{12} and C_{13} constants are the most influenced by the applied pressure and that along their directions the oxide exhibits a stronger resistance to strain. On the other hand, C_{44} reveals a contrary behavior and its value is almost unaffected by pressure.

These same results were obtained by Wang and Ya-Pu [60], using DFT with local (LDA) and gradient-corrected (GGA) functionals as implemented in the CASTEP package, for pressures ranging from 0 to 10 GPa (increment of 2 GPa). They evaluated the cell and internal parameters and also the elastic constants. They likewise showed all elastic constants increase with the pressure, except the C_{44}. Comparing LDA with GGA, the constants calculated with LDA are larger than with GGA. Our values are in better agreement with the experimental data than their results at 0 GPa, and this confirms the dependability of the method applied in the present work.

3.3. Piezoelectric constants

The direct and converse piezoelectric constants of total and clamped-ion contribution are shown in Table 2. At 0 GPa, all the calculated piezoelectric constants presented a good agreement with the experimental data [52,56,58], with a deviation in the order of 14.81%, 23.96%, −18.92% for $\boldsymbol{e}_{31}$, $\boldsymbol{e}_{33}$ and $\boldsymbol{e}_{15}$, and 5.49%, −18.94%, 22.56% for $\boldsymbol{d}_{31}$, $\boldsymbol{d}_{33}$ and $\boldsymbol{d}_{15}$, respectively.

W-ZnO can be easily polarized along the *z*-direction as the structure is strained along that same direction, i.e. the $\boldsymbol{e}_{33} \equiv zzz$ coefficient is the biggest one. A minor induced polarization occurs along *yz* as the strain is applied along *yz*, n_{yz} (e_{15}). In contrast, the major converse piezoelectric response occurs when the electric field is applied along the *yz*-direction which leads to a strain in the same direction ($\boldsymbol{d}_{15}$) while the minor converse piezoelectric response occurs along *xz* ($\boldsymbol{d}_{31}$). Interesting enough, in the ZnO crystal the major piezoelectric response occurs along the most rigid direction. Similar results are reported in previous experimental [57,61] and theoretical studies [14].

The piezoelectric coefficients $\boldsymbol{e}_{31}$, $\boldsymbol{e}_{33}$, $\boldsymbol{e}_{15}$, $\boldsymbol{d}_{31}$, $\boldsymbol{d}_{33}$ and $\boldsymbol{d}_{15}$ become larger as the pressure increases of 42.59%, 33.61%, 34.09%, 62.65%, 63.79% and 63.28%, respectively. The increase of the piezoelectric response along the *z*-direction can be correlated with the internal parameter *u* ($u = d_{ap}/c$, where d_{ap} is the apical Zn–O bond length) and therefore it depends by the Zn and O positions along *z*-direction. However, the clamped-ion piezoelectric coefficients decreases with the pressure of 7.69%, 5.56%, 6.89%, 29.1%, 27.63% and 15.04%, for the $\boldsymbol{e}_{31}$, $\boldsymbol{e}_{33}$, $\boldsymbol{e}_{15}$, $\boldsymbol{d}_{31}$, $\boldsymbol{d}_{33}$ and $\boldsymbol{d}_{15}$, respectively. This difference between the total and clamped-ion constants proves that there is a effect of nuclear relaxation in piezoelectric response.

The overall pressure effect on the piezoelectric properties of W-ZnO is that: (i) ZnO structure becomes more rigid along the *z*-direction, (ii) the direct piezoelectric response is enhanced along this direction and (iii) the converse parameters are more affected by pressure than the direct quantities.

3.4. Topological analyses

The analysis of the topological properties of $\rho(\mathbf{r})$ at the bond critical point (BCP) can provide important information on the pressure effects on the bonding framework. The changes in $\rho(\mathbf{r})$, its Laplacian, the virial and kinetic energy density at the BCP, occurring as the pressure increases, are reported in Table 3. Zn–O interaction was already classified as a "transit" type, neither ionic nor covalent [36], and its character does not change as a function of the loading. As in the case of the geometrical structure, deformations in the charge density are small and do not alter significantly the bonding nature. Nevertheless, a general trend can be envisaged; on one side, $\rho(\mathbf{r})$ and the local energy density increases as an effect of Zn–O distance reduction but, on the other side, the |V|/G ratio decreases and the positive Laplacian increases and these small changes support the hypothesis of a more ionic interplay among the two atoms.

The ellipticity (ε) highlights the shape of the bonds and, under pressure, their directionality tends to zero in proximity of the BCP, which it is compatible with a poor directional interaction such as the case of ionic systems.

As regard the atomic charges, Bader analysis provides data approximately 78% higher than those obtained with the Hirshfeld-I approach. Nevertheless, despite the bad agreement on the absolute values, both QTAIMC and Hirshfeld-I show an increase in the charge transfer from the zinc to the oxygen atom, as a function of pressure and the "stockholder" method results more sensitive. All these features support the hypothesis of a slightly more ionic character of the Zn–O bond under pressure.

In Fig. 2, it is reported the difference between the charge density of the W-ZnO crystal and the isolated atoms, in the plane containing one of the Zn–O bond. As can be seen in Fig. 2, the increase of pressure did not show a significant disturbs on density charge density, which was confirmed by Bader and Hirshfeld-I charges (Table 3) of Zn and O atoms (in absolute values, the positive zinc charge and negative oxygen charge have the same charge value). In percentage, the variations of Zn and O charges are very small when compared with the corresponding variation in bond lengths. Therefore, it can be concluded that the piezoelectricity is more influenced by the shortening of the Zn–O bond, caused by the pressure, than by the charges transfer.

3.5. Electronic properties

In order to understand the influence of pressure on the electronic structure, band structure (Fig. 3) and DOS (Fig. 4) at 12.5 GPa were plotted and compared with their analogous for the

Table 2
Direct ($\boldsymbol{e}$) and converse ($\boldsymbol{d}$) piezoelectric constants of ZnO, in function of pressure, to the total and clamped-ion contribution.

P	*Direct* (C/m^2)			*Converse* (pm/V)		
	e_{31}	e_{33}	e_{15}	d_{31}	d_{33}	d_{15}
			Total			
0.0	−0.54	1.19	−0.44	−4.82	9.97	−10.05
2.5	−0.61	1.29	−0.48	−5.19	10.84	−11.26
5.0	−0.68	1.36	−0.51	−5.90	12.13	−12.52
7.5	−0.71	1.44	−0.54	−6.48	13.41	−13.76
10	−0.77	1.51	−0.57	−7.49	14.87	−15.06
12.5	−0.77	1.59	−0.59	−7.84	16.33	−16.41
			Clamped-ion			
0.0	0.26	−0.54	0.29	1.10	−2.28	4.92
2.5	0.25	−0.53	0.28	1.00	−2.09	4.55
5.0	0.25	−0.52	0.29	0.93	−1.92	4.46
7.5	0.25	−0.52	0.28	0.89	−1.85	4.36
10	0.25	−0.52	0.28	0.84	−1.76	4.26
12.5	0.24	−0.51	0.27	0.78	−1.65	4.18
Exp.	−0.62[a]	0.96[a]	−0.37[a]	−5.10[b]	12.30[b]	−8.20[b]
The.	−0.54[c]	1.19[c]	−0.46[c]	−3.70[c]	8.00[c]	−8.20[c]

[a] [58].
[b] [57,60].
[c] [14].

Table 3
Bond distance ($d_{Zn\text{-}O}$, in Å), variance of bond distance (%Δd) with respect to 0 GPa, distance of each atom from BCP (Å), electron charge density, Laplacian, virial density (V), kinetic energy density (G), |V|/G ratio, and the bond degree H/ρ(r), all in atomic units. The Bader (e_B) and Hirshfeld-I (e_H) charges (in absolute values) were evaluated for Zn and O atoms, and also the variation of the charges (%Δ) with respect to 0 GPa

P	$d_{Zn\text{-}O}$	%Δd	d_{BCP}	d_{BCP}	ρ(r)	$\nabla^2\rho$	G	V	|V|/G	H/ρ(r)	Bader		Hirshfeld-I	
			Zn	O							$\|e_B\|$	$\%\Delta e_B$	$\|e_H\|$	$\%\Delta e_H$
0.0	1.99	0.0	0.96	1.03	0.079	0.419	0.111	−0.117	1.06	−0.075	1.305	0.00	0.729	0.00
2.5	1.98	−0.5	0.96	1.03	0.079	0.427	0.116	−0.122	1.05	−0.077	1.306	0.07	0.732	0.41
5.0	1.98	−0.5	0.95	1.02	0.082	0.444	0.120	−0.126	1.05	−0.077	1.308	0.23	0.732	0.41
7.5	1.96	−1.5	0.95	1.01	0.085	0.474	0.125	−0.131	1.05	−0.078	1.309	0.31	0.733	0.55
10.0	1.95	−2.0	0.94	1.01	0.086	0.488	0.129	−0.136	1.05	−0.078	1.310	0.38	0.734	0.69
12.5	1.95	−2.0	0.94	1.00	0.086	0.490	0.133	−0.140	1.05	−0.079	1.311	0.46	0.735	0.82

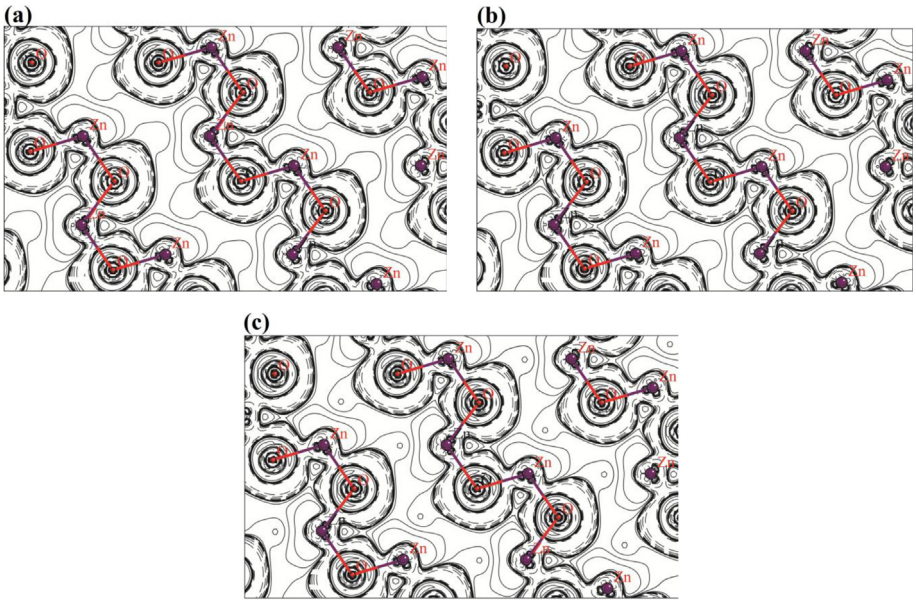

Fig. 2. Electron charge density difference, crystal minus superposition of atoms, (a) 0 GPa, (b) 7.5 GPa and (c) 12.5 GPa. Continuous, dot-dashed and dashed lines represent positive (gain charge), zero and negative (loss charge) values, respectively. A logarithmic scale (−0.1 to 0.1) is used.

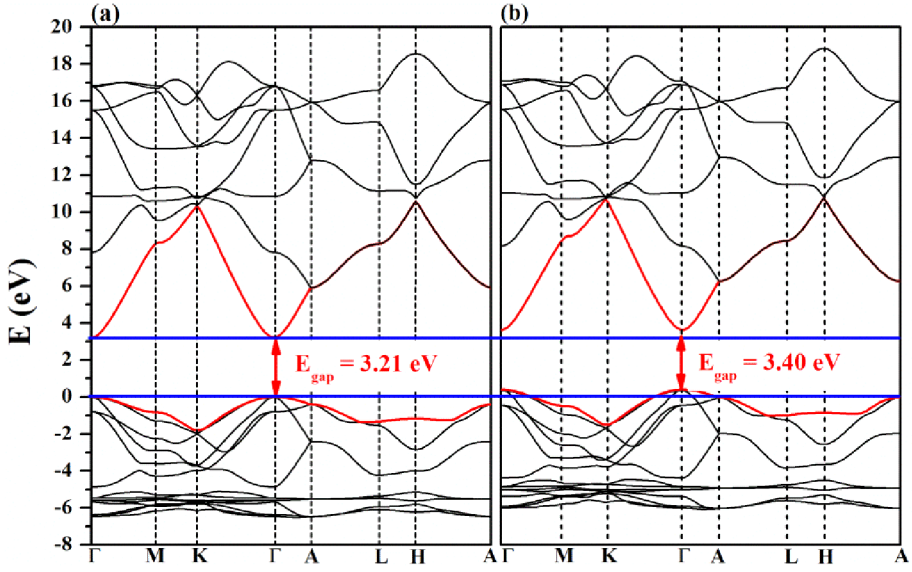

Fig. 3. Band structure of ZnO (a) without pressure and (b) under 12.5 GPa. The blue line corresponds to the top of valence band and bottom of conduct band with respect to the 0.0 GPa.

uncompressed system. In order to easily compare, the zero of the energy was set in accordance with the top of valence band of the crystal at 0 GPa. The band structure and DOS for other pressures are reported in Figs. S1 and S2.

According to Table 1, the E_{gap} presents an increase of 5.92% at 12.5GPa, with respect to its value at 0 GPa. Besides this, the band structure (Fig. 3) is not significantly altered by the pressure, the main features keep unchanged as well as the direct band gap at

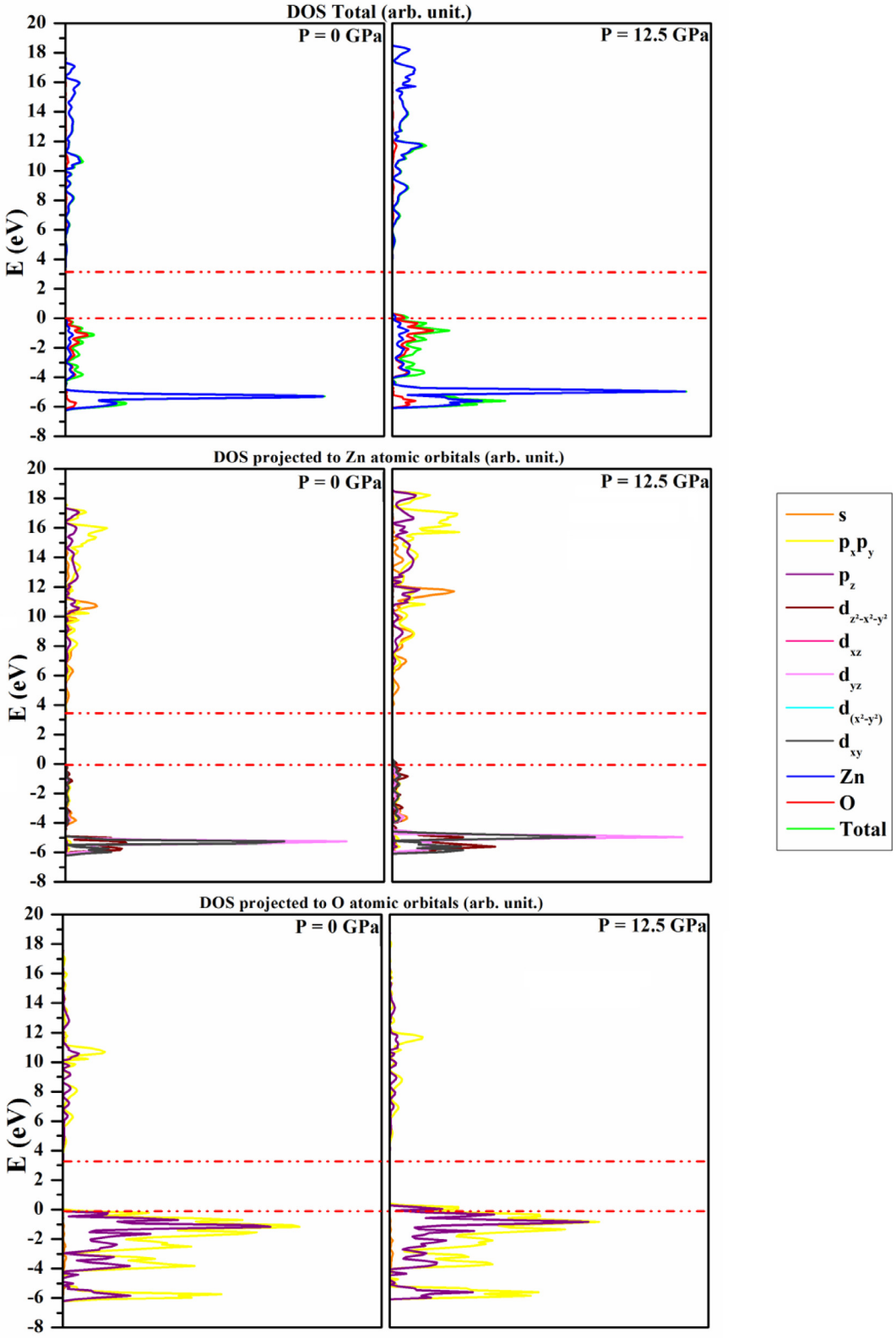

Fig. 4. Density of States of ZnO (a) without pressure and (b) 12.5 GPa. The dashed-dotted red lines correspond to the top of valence band and bottom of conduct band.

Γ-point. On the contrary, the analysis of DOS (Fig. 4) shows the increase of Zn e O atoms contributions at valence band, especially of the 3*d* orbitals of Zn atoms; while at conduct band the contribution had almost the same behavior near the band gap region, presenting an increase in both contributions at inner conduct bands. The contribution of O atoms is maintained near the band gap region and intensified at inner valence band, given that the major contributor is 2*p* orbitals at valence band. Nevertheless, the general contribution of the oxygen and zinc orbitals is kept, with major contribution of $2p_xp_y$ of oxygen at valence band, $3d_{yz}$ of zinc atoms at inner valence band and *s* orbitals of zinc at conduct band in band gap region.

3.6. Vibrational properties

Finally, the IR and Raman spectra of the zinc oxide under pressure are calculated and shown in Fig. 5. The IR and Raman phonon modes, evaluated at 0 GPa and reported in Table 4 for sake of clarity, are in rather good agreement with literature data.

The A mode, active both in IR and Raman spectroscopy, is reproduced with amazing precision as well as the E_1, whose frequency is close to the experimental one but seems absent in the zero pressure structure due to its low intensity.

The discussion of the spectroscopic features deserves some attention. As already stated, the CRYSTAL code keeps the symmetry

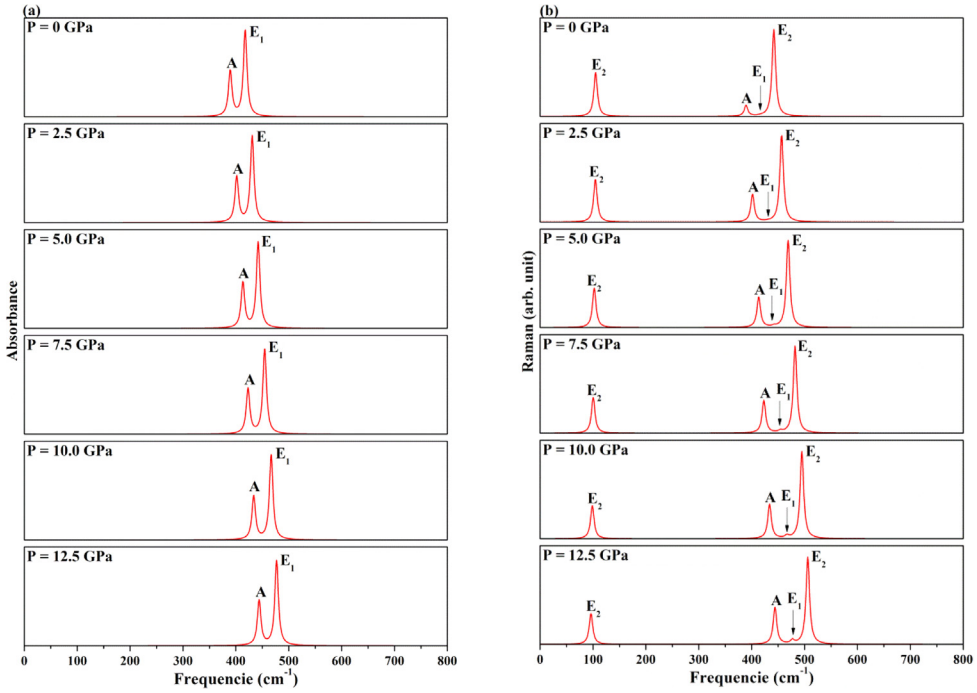

Fig. 5. (a) Infrared and (b) Raman spectrum in function of pressure varies

Table 4
Infrared and Raman active modes (cm^{-1}) for W-ZnO at 0 GPa

		$E_{2\text{-low}}$	$E_{2\text{-high}}$	A	E_1
IR	this work	–	–	389	418
	(exp.) [25]	–	–	389	413
	(exp.) [25]	–	–	380	412
Raman	this work	104	442	389	418
	(exp.) [62]	99	439	382	414
	(theo.) [62]	99	449	397	426

Table 5
Static dielectric constants (parallel ($\epsilon_s^{\parallel}$) and orthogonal ($\epsilon_s^{\perp}$)), and optical dielectric constants (parallel ($\epsilon_o^{\parallel}$) and orthogonal ($\epsilon_o^{\perp}$)).

P	$\epsilon_s^{\parallel}$	$\epsilon_s^{\parallel}$	$\epsilon_s^{\parallel}$	$\epsilon_s^{\parallel}$
0.0	3.23	3.29	1.81	1.80
2.5	3.46	3.34	1.86	1.83
5.0	3.45	3.33	1.86	1.83
7.5	3.44	3.32	1.85	1.82
10	3.43	3.32	1.85	1.82
12.5	3.42	3.30	1.85	1.82
Exp. [55]	3.72	3.68	–	–
The. [17]	3.55	3.38	–	–

of the system, regardless of the pressure applied and this prevents any phase transition from occurring automatically. However, some evidences of structure modifications in the direction of a first-order transition can be noted in IR and Raman spectra. The intensity of the $E_{2\text{-low}}$ mode, around $\sim 100\,cm^{-1}$ in the Raman spectra, decreases with the pressure and its position is down shift of about $96\,cm^{-1}$. The opposite trend is evaluated for the A and E_1 modes: their intensity increases linearly with pressure and the corresponding peaks are up shift. In particular, the total symmetric normal mode A is the most modified one, its frequency shifts from $\sim 389\,cm^{-1}$ at 0 GPa to $\sim 506\,cm^{-1}$ at 12.5 GPa as its intensity is tripled. All these features can be interpreted as a tendency toward a structural rearrangement in order to minimize the stress induced by the applied pressure. This same behavior was also observed experimentally by Decremps and colleagues for both spectra [25,62].

As additional analysis, the static and optical dielectric constants were evaluated through a coupled-perturbed Hartree-Fock/Kohn-Sham (CPHF) scheme [63] adapted to periodic systems [64]. The effect of pressure on dielectric constants are show in Table 5 and compared with the experimental [55] and theoretical [17] values. At 0.0 GPa, the static dielectric constants are in good agreement with experimental and theoretical works, increasing 6.50% and 0.96% to the parallel and orthogonal with respect to the *c* axis, respectively, and the optical dielectric constants increase 2.48% and 1.39%, respectively. Therefore, the static parallel dielectric constant is the most modified by the pressure.

4. Conclusion

The influence of pressure on W-ZnO structural and electronic properties was investigated through DFT/B3LYP calculations. Lattice parameters, volume, elastic constants, energy band gap and IR and Raman features at 0 GPa are in good agreement with literature experimental data.

Several interesting features appear as the pressure is applied. The *c/a* ration is kept although the crystal is more deformed along the *c* than *a* direction. The crystal increases its rigidity; as seen in the bulk modulus evaluation, in particular along the *z*-direction.

Direct and converse piezoelectric responses are intensifying by the pressure: the direct piezoelectric response along the *z*-direction has a maximum when the strain is applied in the same direction, while the major converse piezoelectric response occurs when the electric field is applied along *yz* yielding a strain in the same direction.

On the contrary, band gap and band structure are almost unaffected. As a general conclusion it can be stated that the increase of pressure leads to a more rigid structure, with a major piezoelectric response along to the most rigid direction, *z*.

Finally, both the IR and Raman spectra show significant shift in their major peaks and changes in the relative intensities, phenomena that can be correlated with the initial state of a phase transition.

According to this analysis, zinc oxide can be applied in many electronic and piezoelectric devices, and can support high pressure without changing its electronic and structural properties.

Acknowledgments

This work is supported by Brazilian Funding Agencies: CNPq (46126-4), CAPES PROCAD (88881068492/2014-01), FAPESP (2013/19713-7, 2013/07296-2, 2016/07954-8, 2016/07476-9). The computational facilities were supported by resources supplied by Molecular Simulations Laboratory, São Paulo State University, Bauru, Brazil. Special thanks to the Theoretical Group of Chemistry, Torino University.

Appendix A. Supplementary data

Supplementary data associated with this article can be found, in the online version, at http://dx.doi.org/10.1016/j.chemphys.2017.02.001.

References

[1] D.C. Reynolds, D.C. Look, B. Jogai, Solid State Commun. 99 (1996) 873–875.
[2] H. Sasaki, K. Tsubouchi, N. Chubachi, N. Mikoshib, J. Appl. Phys. 47 (1976) 2046–2049.
[3] Y.G. Wei, C. Xu, S. Xu, C. Li, W.Z. Wu, Z.L. Wang, Nano Lett. 10 (2010) 2092–2096.
[4] M. Law, L.E. Greene, J.C. Johnson, R. Saykally, P.D. Yang, Nat. Mater. 4 (2005) 455–459.
[5] C. Levy-Clement, R. Tena-Zaera, M.A. Ryan, A. Katty, G. Hodes, Adv. Mater. 17 (2005) 1512–1515.
[6] D.-Y. Son, J.-H. Im, H.-S. Kim, N.-G. Park, J. Phys. Chem. C 118 (2014) 16567–16573.
[7] J. Joo, B.Y. Chow, M. Prakash, E.S. Boyden, J.M. Jacobson, Nat. Mater. 10 (2011) 596–601.
[8] S.N. Cha, J.-S. Seo, S.M. Kim, H.J. Kim, Y.J. Park, S.-W. Kim, J.M. Kim, Adv. Mater. 22 (2010) 4726–4730.
[9] B. Kumar, K.Y. Lee, H.-K. Park, S.J. Chae, Y.H. Lee, S.-W. Kim, ACS Nano 5 (2011) 4197–4204.
[10] D. Choi, M.-Y. Choi, W.M. Choi, H.-J. Shin, H.-K. Park, J.-S. Seo, J. Park, S.-M. Yoon, S.J. Chae, Y.H. Lee, S.-W. Kim, J.-Y. Choi, S.Y. Lee, J.M. Kim, Adv. Mater. 22 (2010) 2187–2192.
[11] Z.L. Wang, J.H. Song, Science 312 242–246.
[12] X. Yang, A. Wolcott, G. Wang, A. Sobo, R.C. Fitzmorris, F. Qian, J.Z. Zhang, Y. Li, Nano Lett. 9 (2009) 2331–2336.
[13] U. Ozgur, D. Hofstetter, H. Morkoc, Proc. IEEE 98 (2010) 1255–1268.
[14] M. Catti, Y. Noel, R. Dovesi, J. Phys. Chem. Solids 64 (2003) 2183–2190.
[15] G.H. Zhang, W.J. Chen, J. Zhu, G.L. Jiang, Q. Sheng, B. Wang, Y. Zheng, Aip Adv. 6 (2016), 065217-065217-14.
[16] S.X. Dai, M.L. Dunn, H.S. Park, Nanotechnology 21 (2010).
[17] V. Lacivita, A. Erba, Y. Noel, R. Orlando, P. D'Arco, R. Dovesi, J. Chem. Phys. 138 (2013), 214706-214706-9.
[18] M.H. Zhao, Z.L. Wang, S.X. Mao, Nano Lett. 4 (2004) 587–590.
[19] B. Kumar, S.W. Kim, Nano Energy 1 (2012) 342–355.
[20] N.A. Hill, U. Waghmare, Phys. Rev. B 62 (2000) 8802–8810.
[21] Y. Noel, C.M. Zicovich-Wilson, B. Civalleri, P. D'Arco, R. Dovesi, Phys. Rev. B 65 (2002), 014111-014111-9.
[22] W.F. Perger, J. Criswell, B. Civalleri, R. Dovesi, Comput. Phys. Commun. 180 (2009) 1753–1759.
[23] Y. Noel, M. Llunell, R. Orlando, P. D'Arco, R. Dovesi, Phys. Rev. B 66 (2002), 214107- 214107-8.
[24] J. Serrano, A.H. Romero, F.J. Manjon, R. Lauck, M. Cardona, A. Rubio, Phys. Rev. B 69 (2004), 094306- 094306-14.
[25] J. Pellicer-Porres, A. Segura, V. Panchal, A. Polian, F. Decremps, P. Dumas, Phys. Rev. B 84 (2011), 125202- 125202-6.
[26] A.M. Saitta, F. Decremps, Phys. Rev. B 70 (2004), 035214- 035214-5.
[27] R.F.W. Bader, Atoms in Molecules – A Quantum Theory, Oxford University Press, Oxford, 1990.
[28] C. Gatti, Zeitschrift Fur Kristallographie 220 (5–6) (2005) 399–457.
[29] P. Bultinck, C. Van Alsenoy, P.W. Ayers, R. Carbo-Dorca, J. Chem. Phys. 126 (2007), 144111-144111-9.
[30] A.D. Becke, J. Chem. Phys. 98 (1993) 5648–5652.
[31] C.T. Lee, W.T. Yang, R.G. Parr, Phys. Rev. B 37 (1988) 785–789.
[32] R. Dovesi, R. Orlando, A. Erba, C.M. Zicovich-Wilson, B. Civalleri, S. Casassa, L. Maschio, M. Ferrabone, M. De La Pierre, P. D'Arco, Y. Noel, M. Causa, M. Rerat, B. Kirtman, Int. J. Quantum Chem. 114 (2014) 1287–1317.
[33] J.E. Jaffe, A.C. Hess, Phys. Rev. B 48 (1993) 7903–7909.
[34] T. Bredow, K. Jug, R.A. Evarestov, Phys. Stat. Sol. B 243 (2006) R10–R12.
[35] N.L. Marana, A.R. Albuquerque, F.A. La Porta, E. Longo, J.R. Sambrano, J. Solid State Chem. 237 (2016) 36–47.
[36] N.L. Marana, S.M. Casassa, E. Longo, J.R. Sambrano, J. Phys. Chem. C 120 (2016) 6814–6823.
[37] N.L. Marana, F.A. La Porta, E. Longo, J.R. Sambrano, Curr. Phys. Chem. 5 (2015) 327–336.
[38] R. Dovesi, C. Roetti, R. Orlando, C.M. Zicovich-Wilson, F. Pascale, B. Civalleri, K. Doll, N.M. Harrison, I.J. Bush, P. D'Arco, M. Llunell, M. Causà, Y. Noël, CRYSTAL14 User's Manual, University of Torino, Torino, 2014.
[39] C.M. Zicovich-Wilson, F. Pascale, C. Roetti, V.R. Saunders, R. Orlando, R. Dovesi, J. Comput. Chem. 25 (2004) 1873–1881.
[40] C. Gatti, S. Casassa, TOPOND user's manual, TOPOND user's manual (2013).
[41] R.F.W. Bader, Am. Chem. Soc. 207 (1994) 246.
[42] P.L.A. Popelier, Chem. Phys. Lett. 228 (1994) 160–164.
[43] F.L. Hirshfeld, Theor. Chim. Acta 44 (1977) 129–138.

[44] C.M. Zicovich-Wilson, M. Ho, A.M. Navarrete-Lopez, S. Casassa, Theor. Chem. Acc. 135 (2016) 1–13.
[45] K. Doll, Mol. Phys. 108 (2010) 223–227.
[46] A. Erba, A. Mahmoud, R. Orlando, R. Dovesi, Phys. Chem. Miner. 41 (2014) 151–160.
[47] R. Resta, Rev. Mod. Phys. 66 (1994) 899–915.
[48] G. Sághi-Szabó, R.E. Cohen, First-principles study of piezoelectricity in PbTiO3, Phys. Rev. Lett. 80 (10) (1998) 4321–4324.
[49] A. Mahmoud, A. Erba, K.E. El-Kelany, M. Rerat, R. Orlando, Phys. Rev. B 89 (2014), 045103- 045103-9.
[50] F. Decremps, F. Datchi, A.M. Saitta, A. Polian, S. Pascarelli, A. Di Cicco, J.P. Itie, F. Baudelet, Phys. Rev. B 68 (2003), 104101- 104101-10.
[51] R.C. Lima, L.R. Macario, J.W.M. Espinosa, V.M. Longo, R. Erlo, N.L. Marana, J.R. Sambrano, M.L. dos Santos, A.P. Moura, P.S. Pizani, J. Andres, E. Longo, J.A. Varela, J. Phys. Chem. A 112 (2008) 8970–8978.
[52] J.M. Calleja, M. Cardona, Phys. Rev. B 16 (1977) 3753–3761.
[53] J.F. Nye, Physical Properties of Crystals, Dover Publication, New York, 1957.
[54] G. Ottonello, B. Civalleri, J. Ganguly, W.F. Perger, D. Belmonte, M.V. Zuccolini, Am. Mineral. 95 (2010) 563–573.
[55] U. Ozgur, Y.I. Alivov, C. Liu, A. Teke, M.A. Reshchikov, S. Dogan, V. Avrutin, S.J. Cho, H. Morkoc, J. Appl. Phys. 98 (2005), 041301- 041301-103.
[56] S. Desgreniers, Phys. Rev. B 58 (1998) 14102–14105.
[57] L. Bornstein, Group III: Solid State Physics, Low Frequency Properties of Dielectric Crystals: Piezoelectric, Pyroelectric and Related Constants, Springer, Berlin, 1993, pp. 330–332.
[58] L. Bornstein, Numerical Data and Function Relationships: Sciences and Technology, Springer, Berlin, 1979.
[59] J.E. Jaffe, J.A. Snyder, Z.J. Lin, A.C. Hess, Phys. Rev. B 62 (2000) 1660–1665.
[60] . Wang, Z. Ya-Pu, A Density Functional Study of Zinc Oxide Elastic Properties Under High Pressure, IUTAM Symposium on Surface Effects in the Mechanics of Nanomaterials and Heterostructures 31 (2012) 229-245.
[61] E.E. Tokarev, I.B. Kobyakov, I.P. Kuz'mina, A.N. Lobachev, G.S. Pado, Sov. Phy. Solid State 17 (1975) 629–632.
[62] F. Decremps, J. Pellicer-Porres, A.M. Saitta, J.C. Chervin, A. Polian, Phys. Rev. B 65 (2002), 092101- 092101-4.
[63] G.J.B. Hurst, M. Dupuis, E. Clementi, J. Chem. Phys. 89 (1988) 385.
[64] B. Kirtman, F.L. Gu, D.M. Bishop, J. Chem. Phys. 113 (2000) 1294.